Seismic structures in the Earth's inner core below Southeastern Asia

P.B. Kaazik, Krasnoshchekov D.N, Ovtchinnikov V.M.

Institute of Dynamics of Geospheres, Russian Academy of Sciences, Moscow, Russia, krasnd@idg.chph.ras.ru

1. DATA

We analyze 292 polar ($26° < \xi < 33°$ and $2° < \xi < 15°$) measurements from stations SYO, SNAA, MAW, P061, LONW, 60 Fennoscandian stations of LAPNET array, as well as ARCESS, FINES and Spitsbergen arrays. Sources are around Aleutian and Kurile Islands, in Western Siberia and Arctics, at Novaya Zemlya and New Zealand (Fig. 1). Polar paths sample "quasi-eastern" hemisphere of the IC beneath Australia and Southeastern Asia. 133 equatorial measurements ($44° < \xi < 65°$) come from Fiji events recorded by European and Near East stations. Our dataset provides tight sampling of the IC between 90°E and 135°E by both polar and equatorial paths.The IC surface enter/exit points of the crossing PKP_{DF} polar and equatorial rays are distributed over the area of about 800x1200 km (Fig. 2). The relevant PKP_{DF} bottom refraction points stretch mostly in North-East direction, and a significant their part is localized in a small volume of 200x400x200 km where polar and equatorial waveforms undergo refraction in nearly the same place. Only unambiguous DF and BC arrivals (Fig. 3) were used for manual travel time picking (between their same polarity amplitude maxima). No cross-correlation was necessary.

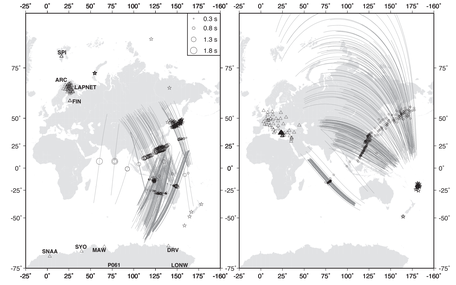

Fig. 1. World map with projections of the analyzed polar (left) and equatorial (right) PKP_{DF} ray segments in the inner core on daylight surface. Triangles denote locations of seismic stations and arrays, stars – locations of the analyzed seismic events. The triangles in precise locations of Antarctic stations LONW and P061 at latitudes of -81.3° and -84.5° are beyond the south high latitudes limit of the map. The circles denoting absolute PKP_{BC}–PKP_{DF} differential travel time residuals are located at the respective PKP_{DF} turning points. The polar circles' radii are proportional to the absolute differential travel times in conformity with the scale in the upper right corner.

Fig. 2. The globe with projections of the analyzed PKP_{DF} ray segments in the inner core on daylight surface. Equatorial paths are green, polar are ginger (LAPNET data) and yellow (SYO, SNAA). Triangles are locations of PKP_{DF} equatorial bottom refraction points in the IC. Circles are polar turn points scaled proportionally to the absolute value of residuals.

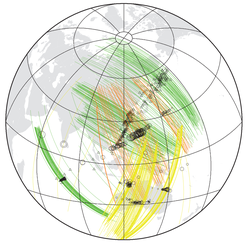

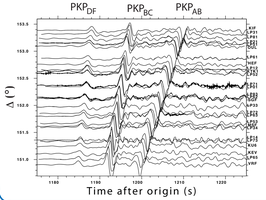

Fig. 3. Plot record section of the event occurred to the south of New Zealand (latitude: -49.1704, longitude: 164.4230, focal depth 18 km) on 30/09/2007 at 09:47:53.41. Raw records of broadband vertical channels belong to stations of LAPNET array (station codes are on the right side).

2. MEASUREMENTS

To allow for lower mantle effects, we calculated corrections with respect to global three-dimensional tomographic cell model MITP08. The majority of mantle corrections never exceeded 0.1 s in abs value (Fig. 4). The whole dataset of differential travel times is obviously inconsistent with a simple model of uniform cylindrical anisotropy (see the the measured dependence of τ on ξ in Fig. 5). Pronounced lateral changes in isotropic velocity can be also ruled out. This is because such heterogeneity is to affect both polar and equatorial paths (in case they probe essentially the same volume of the IC), but the observed scatter in polar data (perpendicular to the assumed gradient) turns out few times as big as the one in the equatorial data (along the assumed gradient). The residuals dependence on PKP_{DF} turning depth H_{max} below the ICB (Fig. 6) is peculiar too. The region of shallow turning depths is characterized by no difference between the equatorial and polar residuals and hence can be called isotropic. By eye, the residuals distinctly diverge only below 225 km – the apparent depth of transition from isotropy to anisotropic bulk IC. However the picture of depth dependence is not conclusive since lots of polar measurements are still among the equatorial ones even below the depth of 225 km.

Fig. 4. The dependence of PKP_{BC}–PKP_{DF} differential travel time residuals ($\tau_{mea} - \tau_{ak135} + \tau_{man}$) in seconds on epicentral distance (Δ) in degrees. Closed circles – PKP residuals before correction for mantle heterogeneities, open circles – corrected PKP residuals.

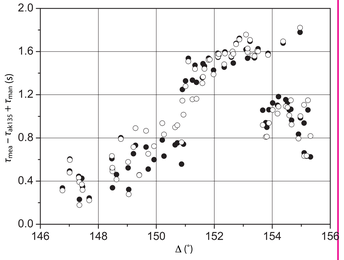

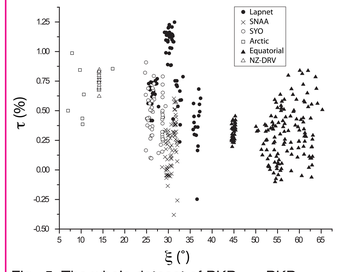

Fig. 5. The whole dataset of PKP_{BC}–PKP_{DF} differential travel time residuals (τ) plotted versus PKP_{DF} ray angle with the Earth's rotation axis (ξ) in the inner core. Subsets corresponding to different stations or paths are denoted by different signs (see the legend in the upper right corner).

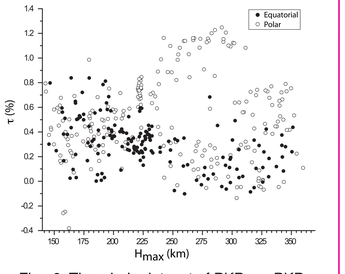

Fig. 6. The whole dataset of PKP_{BC}–PKP_{DF} differential travel time residuals (τ) plotted versus PKP_{DF} turning depth under the ICB (H_{max}). White circles correspond to polar paths, black circles – to the equatorial paths.

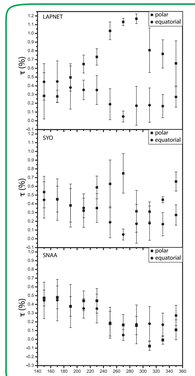

Fig. 7. Equatorial and polar averaged residuals binned for 20 km depth of PKP_{DF} bottom refraction point below the ICB. The data subset name is in the upper left corner. Error bars indicate the standard deviation of the average residual for each bin.

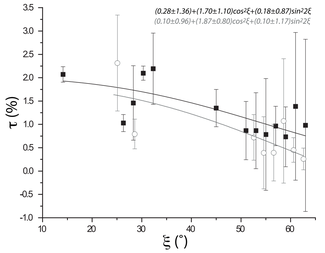

3.1 INTERPRETATION. LAYERED MODEL.

The easiest way to explain the observed obscure divergence of polar and equatorial residuals is to invoke a simple model where the isotropy-anisotropy transition increases/decreases with depth in the observation area. The collected polar residuals in Fig. 7 sample three nearby regions of the IC. The PKP_{DF} traces to SNAA probe the upper IC volume below central and western Australia, to SYO – beneath northern Australia and off its coast, and LAPNET data correspond to South China Sea and Philippines (Fig. 1 and 2). The three regions of the profile stretching mostly to East from Asian coast are divided in the core by approximately 600 and 240 km. This allows tracking changes in contrastive patterns of depth dependence of polar and equatorial residuals along the profile. The presented data can be considered complementary to each other and thus produce the smooth picture best explainable by spatial changes in the isotropy depth. The thickness of IC isotropic roof can vary from 190 km (LAPNET data) to 360 km (SNAA data). To estimate the strength of underlying anisotropy in this model we fit the anisotropic model curve to LAPNET and SYO differential travel time residuals (Fig. 8). Both LAPNET and SYO least squared curves produce essentially the same shape with close parameters, which is a characteristics of the local IC fabric

Fig. 8. Fitting the anisotropy model curve to LAPNET (black) and SYO (grey) subsets. The results and error of least squares fit are given in the upper right corner. LAPNET dataset was enhanced with DRV measurements ($\xi = 14°$) that had nearby PKP_{DF} bottom refraction points (see Fig. 1).

3.2 INTERPRETATION. LOCAL HETEROGENEITY.

Another viable model capable of fitting the data is local heterogeneity. It is roughly visualized by residuals in Fig. 9. The area of increased residuals at LAPNET is quite distinct and restricted to depths below 225 km, in the range of North latitudes from 18° to 23° and East longitudes from 125° to 135°. Polar residuals without the increased LAPNET data vary from almost zero to +0.8% with mean (0.4 ± 0.2) % averaged over 174 datapoints. The compact volume of stronger anisotropy is probed by 33 polar rays that yield residuals between 0.88% and 1.24% with mean (1.10 ± 0.09)%. Constraining the assumed anisotropic heterogeneity isn't straightforward because at least three parameters remain to be estimated on the base of the available measurements. The anomaly size appears to be not large, so its anisotropic strength defined by iron crystal texture must not reveal significant spatial changes. On the contrary, its fast anisotropy axis is easy to imagine in almost any direction. Another uncertain parameter of the anomaly is the depth of its top under the ICB. Reasonable trade-offs between these parameters may increase ambiguity and add more model non-uniqueness. We picked the model described in Fig. 10 because it minimized variation in anisotropy strength w.r.t. different positions of the anomaly top, helping to justify its small size. The fast anisotropy direction is assumed along the spin axis, so our PKP_{DF} beams propagate in it at $\xi \approx 30°$. We then validated the velocity model relevant for such anisotropic heterogeneity and $\xi \approx 30°$ by evaluating synthetic waveforms of PKP_{BC} and PKP_{DF} branches (Fig. 11).

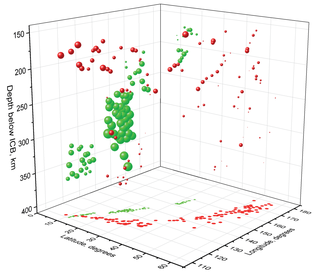

Fig. 9. Polar residuals measured at LAPNET (green balls) and all equatorial residuals (red balls) jointly plotted in locations of their respective PKP_{DF} refraction points in the inner core. Green and red dots on the bottom plane are the balls' projections onto the surface of constant depth of 420 km below the ICB.

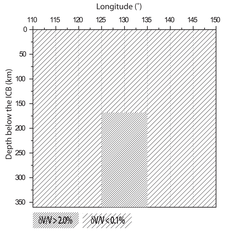

Fig. 10. Cross section of the anisotropic structure in the top of the inner core along the profile probed by the LAPNET residuals.

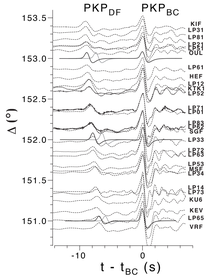

Fig. 11. Plot record section of synthetic seismograms overlaid with raw traces of LAPNET (dash) from Fig. 3. Black trace corresponds to synthetic PKP waveforms evaluated for polar paths through the suggested anisotropic anomaly in the IC at $\xi \approx 30°$, grey is for PKP_{DF} in ak135.

4. CONCLUSIONS

We have analysed a new dataset of polar and equatorial PKP differential travel times. It consists of high quality hand picked measurements made over the seismic paths sampling the IC below Southeastern Asia and Australia. The contrastive patterns of depth dependence of polar and equatorial residuals observed below Asia and Australia can be accounted for by a layered model where the isotropy-anisotropy transition is 190 km below the ICB under Asia and about 350 km under Australia. This dipping in South-East direction discontinuity is between the isotropic top of the IC and its almost 2% anisotropic body. The data produce some evidence for dominance of cylindrically ordered cubic shaped iron crystals in the sampled anisotropic volume of the IC. However the interpretation is not unique. Spatial distribution of the residuals suggests separation of a group of 33 LAPNET measurements that exhibit increased values comparing to the rest of the dataset and sample a restricted IC volume below Southeastern Asia. The split interpretation of the dataset yields almost isotropic (<0.1%) eastern hemisphere of the IC at least down to the depth of 360 km with presence of small volume of strong anisotropy (more than 2%). It is localized at depths below 170 km under the ICB, and restricted by the ranges of 18°-23° and 125°-135° of North latitude and East longitude, accordingly. Each model (layered or local heterogeneity) has its counterpart in previous studies of the Earth's core and feasible physical mechanism to be caused by. However interpreted, the presented differential travel time residuals reveal a new seismic structure compounded of the media exhibiting fast changes in anisotropic properties. Further effective pursuit of the models presents challenges in terms of resolution and coverage and basically requires a significant dataset extension.

5. ACKNOWLEDGEMENTS

The POLENET/LAPNET project was a part of the International Polar Year 2007-2009 and a part of the POLENET IPY consortium. Organizations participated in the POLENET/LAPNET project are: (1) Sodankylä Geophysical Observatory of the University of Oulu (Finland), (2) Institute of Seismology of the University of Helsinki (Finland), (3) University of Grenoble (France), (4) University of Strasbourg (France), (5) Institute of Geodesy and Geophysics, Vienna University of Technology (Austria), (6) Geophysical Institute of the Czech Academy of Sciences, Prague (Czech Republic), (7) Institute of Geophysics ETH Zürich (Switzerland), (8) Institute of Geospheres Dynamics of the Russian Academy of Sciences, Moscow (Russia), (9) The Kola Regional Seismological Centre, of the Russian Academy of Sciences (Russia), (10) Geophysical Centre of the Russian Academy of Sciences, Schmidt Institute of Physics of the Earth of the Russian Academy of Sciences (Russia), (11) Swedish National Seismological Network, University of Uppsala (Sweden), (12) Institute of Solid Earth Physics, University of Bergen (Norway), (13)NORSAR (Norway), (14) University of Leeds (UK). Equipment for the temporary deployment was provided by RESIF - SISMOB, FOSFORE, EOST-IPG Strasbourg Equipe ismologie (France), seismic pool (MOBNET) of the Geophysical Institute of the Czech Academy of Sciences (Czech republic), instrument pool of Sodankylä Geophysical Observatory (Finland), Institute of Geosphere Dynamics of RAS (Russia), Institute of Geophysics ETH Zürich (Switzerland), Institute of Geodesy and Geophysics, Vienna University of Technology (Austria), University of Leeds (UK). Funding agencies provided support for organization of the experiment are: Finland : The Academy of Finland (grant No. 122762) and University of Oulu France: BEGDY program of the Agence Nationale de la Recherche, Institut Paul Emil Victor and ILP (International Lithosphere Program), task force VIII. Czech Republic grant No. IAA300120709 of the Grant Agency of the Czech Academy of Sciences Russian Federation : Russian Academy of Sciences (programs No 5 and No 9). POLENET/LAPNET Working Group: Elena Kozlovskaya (1), Helle Pedersen (3), Jaroslava Plomerova (6), Ulrich Achauer (4), Eduard Kissling (7), Irina Sanina (8), Teppo Jämsen (1), Hanna Silvennoinen (1), Catherine Pequegnat (3), Riitta Hurskainen (1), Robert Guiguet (3), Helmut Hausmann (5), Petr Jedlicka (6), Igor Aleshin (10), Ekaterina Bourova (3), Reynir Bodvarsson (11), Evald Brückl (5), Tuna Eken (6), Pekka Heikkinen (2) Gregory Houseman (14), Helge Johnsen (12), Elena Kremenetskaya (9), Kari Komminaho (2), Helena Munzarova (6) Roland Roberts (11), Bohuslav Ruzek (6), Hossein Shomali (11), Johannes Schweitzer (13), Artem Shaumyan (8), Ludek Vecsey (6), Sergei Volosov (8).